Mathematical Model for Dropwise Condensation on a Surface With Wettability Gradient

Manjinder Singh
Department of Mechanical Engineering,
Indian Institute of Technology Delhi,
Hauz Khas 110016, New Delhi, India

Sasidhar Kondaraju
School of Mechanical Sciences,
Indian Institute of Technology Bhubaneswar,
Bhubaneswar 751013, Orrisa, India

Supreet Singh Bahga[1]
Department of Mechanical Engineering,
Indian Institute of Technology Delhi,
Hauz Khas 110016, New Delhi, India
e-mail: bahga@mech.iitd.ac.in

We present a mathematical model for dropwise condensation (DWC) heat transfer on a surface with wettability gradient. We adapt well-established population balance model for DWC on inclined surfaces to model DWC on a surface with wettability gradient. In particular, our model takes into account the effect of wettability gradient and energy released during drop coalescence to determine the drop departure size. We validate our model with published experimental data of DWC heat flux and drop size distribution. Based on various experimental studies on drop motion, we also propose a mechanism that explains how the energy released during drop coalescence on a surface with wettability gradient and in a condensation environment aids drop motion. The mechanism correctly explains the shift of center of mass of two coalescing drops on a surface with wettability gradient toward the drop on high wetting region. Using the model, we analyze the effect of wettability gradient on the DWC heat flux. Our model predictions show that the optimal choice of wettability gradient is governed by differential variations in population density and heat transfer through a drop with change in wettability of the surface. We also demonstrate that contact angle at which there is maximum heat transfer through a drop varies with thickness of coating layer leading to change in optimal wettability gradient. [DOI: 10.1115/1.4039014]

1 Introduction

Condensation of vapor on a surface is classified as either filmwise condensation (FWC) or dropwise condensation (DWC) [1–3]. In FWC, a thin liquid film of condensate covers the entire surface and act as an additional layer of resistance to heat transfer, whereas, in DWC, vapor condenses into small droplets, which are removed periodically. Because of lower thermal resistance of discrete drops compared with a continuous film, DWC provides an order of magnitude higher heat transfer rate than FWC [1–3]. However, ideal DWC occurs only at low values of temperature difference ΔT (termed as degree of subcooling) between surface and saturated vapor. As the degree of subcooling is progressively increased, condensation first transitions to mixed mode consisting of partial DWC and partial FWC [4–7]. At sufficiently high values of degree of subcooling, condensation becomes completely filmwise [4–7].

The efficiency of DWC primarily depends on the rate at which condensate drops are removed and bare surface is generated (surface renewal rate) for fresh condensation cycle. This is because higher surface renewal rate results in smaller droplets and correspondingly higher droplet density. Typically, spontaneous removal of condensate drops is achieved by inclining the condensing surface which causes drops to fall under the action of gravity. However, due to contact angle hysteresis [8], droplets have to grow to the size of capillary length [9] before being spontaneously removed by gravity. For further improvement of DWC heat transfer, one needs to employ a droplet removal mechanism capable of initiating spontaneous motion of droplets at length scales smaller than the capillary length.

Recent studies by Daniel et al. [10] and Macner et al. [11] have shown that, on a surface with wettability gradient, condensed drops move spontaneously from low to high wetting region. The spontaneous motion results from surface energy gradient and excess surface energy released during drop coalescence. On a horizontal surface with continuous radial wettability gradient, Daniel et al. observed rapid motion of condensate drops. Compared to FWC, Daniel et al. reported an order of magnitude higher rate of heat transfer. In a similar experiment, Macner et al. [11] observed that condensation on surface with wettability gradient shifts the drop size distribution toward smaller size drops and lowers the fraction of area covered by liquid when compared with uniformly hydrophobic surface. The use of a surface with wettability gradient for removal of condensed drops is particularly interesting because it can enhance drop removal rate over and above the drop removal rate obtained by inclining the surface. Moreover, wettability gradient provides a way to achieve dropwise condensation for applications in gravity free environment and on horizontal surfaces. Such wettability gradients can be generated on a variety of surfaces such as silane diffusion on silicon wafers [12], contact printing of octadecyltrichlorosilane on oxidized silicon wafers [13], and using alkali surface oxidation and laser etching of copper [14,15].

In DWC, drops form on surface cavities known as nucleation sites [8,16,17] and following which these drops grow. The growth of drops has been categorized into two phases: small drops and large drops [8,16–18]. In the initial phase, drops grow primarily by direct condensation of vapor on its surface (referred here as small drops). Later, when the drops become large and space between neighboring drops becomes small, growth due to coalescence starts dominating (referred here as large drops). And finally, when the drops grow to a size large enough to be removed, they depart from the condensing surface regenerating the surface in the process for fresh condensation cycle. As a result, drop size has a continuous distribution from some minimum value, as defined by thermodynamic limit [19], up to a size at which drops depart from the condensing surface.

While there have been several experimental studies [10,11,20] demonstrating the effect of wettability gradient on DWC heat

[1]Corresponding author.

Contributed by the Heat Transfer Division of ASME for publication in the Journal of Heat Transfer. Manuscript received May 5, 2017; final manuscript received January 4, 2018; published online April 6, 2018. Assoc. Editor: Debjyoti Banerjee.

transfer, there is no corresponding mathematical model for predicting DWC heat transfer rate on a surface with wettability gradient. Previous models for DWC are limited to vertical surfaces wherein condensed drops are removed by gravity. In these studies, the drop departure size is governed by the balance of hysteresis force and gravity. In contrast, on a wettability gradient surface, drops are removed by the force due to wettability gradient. To best of our understanding, none of the earlier models for DWC account for force due to wettability gradient for removal of condensed drops.

In this paper, we present a mathematical model to predict the condensation performance of surface with wettability gradient under ideal DWC conditions. We use population balance model initially proposed by Tanaka [16] and refined later by Abu-Orabi [18] for DWC on an inclined surface. In the model, heat transfer through a single drop of radius r is combined with its respective number density to obtain the DWC heat flux. The efficacy of the model primarily relies on accurate prediction of maximum and minimum drop size. While the minimum drop size $r_{\min}$ is defined by thermodynamic limit [19], the maximum drop size $r_{\max}$ depends on balance of hysteresis force by the force responsible for droplet removal from the condensation surface.

In the current work, we find the maximum size of the condensed drops by balancing the driving force on drops due to wettability gradient with hysteresis force. More importantly, we take into account the effect of coalescence released surface energy in overcoming the hysteresis force. We also describe the mechanism by which coalescence released surface energy aids the motion of the condensed drops on a surface with wettability gradient. We validate our model with the published experimental data of DWC heat flux [21] and drop size distribution [11] obtained for surface with wettability gradient. Thereafter, we show the effect of wettability gradient on the DWC heat flux. Our model predictions show that DWC heat flux first increases and then decreases with an increase in wettability gradient. Finally, we show the effect of coating layer and demonstrate that optimal choice of wettability gradient depends on the thickness of coating layer.

2 Mathematical Modeling

We here present a population balance model to predict condensation heat transfer on a wettability gradient surface. In this model, we make several simplifying assumptions. First, we assume that the drop size distribution remains statistically steady over the entire condensing surface. This assumption is routinely employed in DWC modeling and has been validated experimentally [11,22,23]. Second, convective heat transfer between vapor and surface is negligible as compared with latent heat of condensation h_{fg}. Therefore, we assume that there is no heat transfer between the vapor and the uncovered surface in between the drops and all heat flows through the base of the drops. As $\mathrm{Nu} \ll 1$ within the drop, we neglect the convection effects and assume that conduction is the dominant mode of heat transfer.

As described in Sec. 1, the growth of drops can be divided into two phases: (i) small drops, which grow due to direct condensation and (ii) large drops, which grow due to coalescence. Figure 1 shows a typical drop size distribution in DWC consisting of small drops and large drops. For steady drop size distribution, condensation heat transfer on a unit surface area is equal to heat transfer through a single drop times the respective number density and is expressed as

$$Q'' = \int_{r_{\min}}^{r_e} q_d(r) n(r) dr + \int_{r_e}^{r_{\max}} q_d(r) N(r) dr \tag{1}$$

where $n(r)$ and $N(r)$, respectively, are number of small and large drops per unit area per unit radius around r. The minimum drop radius $r_{\min} = 2\gamma T_{\mathrm{sat}}/h_{fg}\rho\Delta T$ [19], where γ and ρ, respectively, denote surface energy and density of the liquid, and T_{sat} represent saturation temperature. The radius r_e, as shown in Fig. 1, denotes

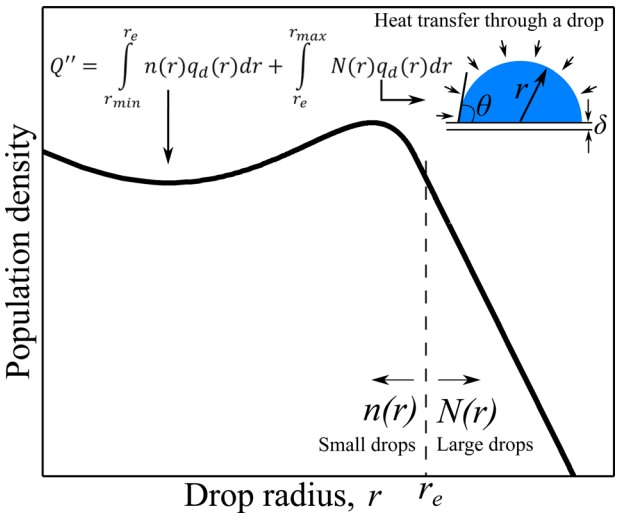

Fig. 1 Schematic showing drop size distribution in DWC. Drop size distribution is divided Into two phases small drops $n(r)$ and large drops $N(r)$. The drop radius r_e denotes boundary between small and large drops.

drop radius at the boundary between small and large drops and q_d denotes heat transfer through a drop of radius r.

2.1 Heat Transfer Through a Single Drop. Determination of heat transfer through a body requires knowledge of all contributing thermal resistances. Heat transfer through a drop involves convection at liquid–vapor interface and conduction between drop and condensation surface. Therefore, there is convection resistance at the interface and conduction resistance due to drop itself. In addition, there are resistances due to coating layer and curvature of the drop (Kelvin effect) [8,18]. By taking into account all the resistances, Kim and Kim [8] have provided following expression for heat transfer through a drop q_d of radius r:

$$q_d = \frac{\Delta T \pi r^2 \left(1 - \dfrac{r_{\min}}{r}\right)}{\dfrac{\delta}{K_{\mathrm{coat}} \sin^2\theta} + \dfrac{r\theta}{4K_c \sin\theta} + \dfrac{1}{2h_i(1-\cos\theta)}} \tag{2}$$

Here, θ is the contact angle, δ is the thickness of the coating layer, $h_i = 15.7\,\mathrm{MWm^{-2}K^{-1}}$ at 1 atm [8] is interfacial heat transfer coefficient, and K_c and K_{coat} represent thermal conductivity of water and coating layer, respectively.

2.2 Drop Size Distribution. To predict the drop size distribution of small drops, which grow mainly by direct condensation, we use population balance model similar to previous DWC studies on inclined surfaces [8,16,18,23]. We consider an arbitrary droplet radius range $r_1 -$ to $- r_2$. For conservation of number of drops in this radius range, number of drops entering by growth equals the number of drops leaving by growth plus the number of drops being swept away by large departing drops. This equilibrium in the limit $\Delta r \to 0$ ($\Delta r = r_2 - r_1$) can be expressed as [8,16,18,23]

$$\frac{d}{dr}(Gn) + \frac{n}{\tau} = 0, \quad G = \frac{dr}{dt} \tag{3}$$

where G is the growth rate and τ is the sweeping period. The sweeping period $\tau = A/S$, where A is the area of an arbitrary part of the condensing surface and S is the rate at which surface is renewed by droplets in motion.

The time-scale of heat conduction, $t_c = r^2/\alpha$ (α is thermal diffusivity), through a drop is very small ($\sim\mathcal{O}(1\,\mu\mathrm{s})$) as compared to

the time-scale of droplet growth, $t_g = \rho h_{fg} r/(h\Delta T)$ ($\sim \mathcal{O}(1\,\text{ms})$) [2] ($h$ is heat transfer coefficient). Therefore, under the quasi-steady-state heat conduction approximation, the rate of heat transfer q_d through a drop of radius r can be equated to rate of condensation of vapor on drop surface. From the above approximation and assuming constant contact angle growth of condensing drop, we get heat transfer through a drop q_d in terms of droplet growth rate G as [24]

$$q_d = \rho h_{fg} \pi r^2 (2 - 3\cos\theta + \cos^3\theta) G \tag{4}$$

Equating Eqs. (2) and (4), we get G as a function of r. Using the resulting relation in Eq. (3) and integrating, we get appropriate governing equation [8] for drop size distribution of small drops. The constant of integration is found using boundary condition $n(r_e) = N(r_e)$. The drop size distribution of large drops $N(r)$ is given by the distribution function proposed by Le Fevre and Rose [25] as

$$N(r) = \frac{1}{3\pi r^2 r_{\max}} \left(\frac{r}{r_{\max}}\right)^{-2/3} \tag{5}$$

where the maximum drop size $r_{\max}$ is determined from balance of hysteresis by the force driving the drops.

2.3 Maximum Drop Size. In conventional arrangement, condensation surfaces are inclined to affect gravity operated removal of condensed drops. In such cases, $r_{\max}$ is equal to capillary length scale ($r = \sqrt{\gamma/\rho g}$). In the current work, we consider a horizontal surface, which is treated chemically to obtain continuous contact angle variation with position x. On such a surface and in the absence of condensation, drops move when force due to wettability gradient exceeds the hysteresis force. At the instant when drop just begins to move force due to wettability, gradient is balanced by hysteresis force, as described by Daniel and Chaudhury [26]

$$\pi r_b^2 \gamma \frac{d(\cos\theta_d)}{dx} - 2\gamma r_b (\cos\theta_{r,o} - \cos\theta_{a,o}) = 0 \tag{6}$$

where the subscript o denotes center of the drop and subscripts a and r denote advancing contact angle (ACA) and receding contact angle (RCA) of the drop, respectively. In Eq. (6), r_b denotes base radius of the drop and subscript d denotes macroscopic dynamic contact angle defined as $\cos\theta_d = (\cos\theta_a + \cos\theta_r)/2$. First and second terms on the right-hand side of Eq. (6) denote force, due to wettability gradient, and hysteresis, respectively. Solving Eq. (6), we get droplet base radius r_b at which the drops begin to move. However, in the condensation environment, Zhao and Beysens [20] observed that center of mass of coalescing drops, which otherwise are immobile, shifts toward the hydrophilic region. Daniel et al. [10] reported similar observations with the exception that the merged drop started moving toward the high wetting region. This motion of merged drop toward the hydrophilic region was attributed to energy released due to coalescence and direct condensation of vapor on droplet surface. Therefore, in the condensation environment, the force due to wettability gradient is aided by two additional factors in overcoming the hysteresis force: (i) energy released due to coalescence with other drops and (ii) by direct condensation of vapor on droplet surface [10].

To take the effect of coalescence into account, we propose a mechanism of droplet coalescence in a condensation environment on a surface with wettability gradient which, in part, is based on the mechanism previously proposed by Daniel et al. [10]. The proposed mechanism is illustrated schematically in Fig. 2. The overall effect of coalescence can be considered as pumping of liquid from the drop on low wetting region to the drop on high wetting region leading to unpinning of contact line, as shown in Fig. 2. To describe the mechanism, we first consider separate effects of wettability gradient and condensation of vapor on the dynamic contact angle of a drop before combining the two to give a full depiction.

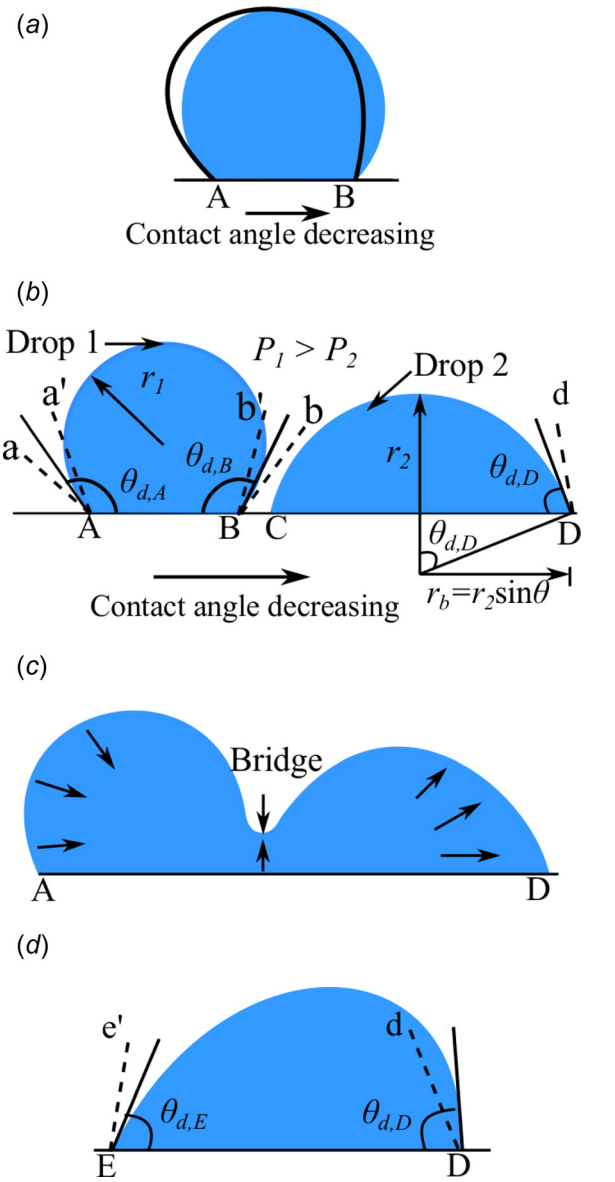

Fig. 2 Schematic illustrating the mechanism of coalescence of two drops on a surface with wettability gradient. *P* denotes Laplace pressure and r_b denotes base radius of the drop. Solid lines show dynamic contact angles at respective drop edges ($\theta_{d,A}, \theta_{d,B}, \theta_{d,D}$, and $\theta_{d,E}$). The dashed lines denote receding ($\angle b'BA$, $\angle a'AB$, and $\angle e'ED$) and advancing ($\angle bBA$, $\angle aAB$, and $\angle dDE$) contact angle at respective drop edges. (*a*) Shifting of drop shape from staggered to nearly spherical cap shape on a surface with wettability gradient in the absence of condensation. (*b*) State of a drop on a surface with wettability gradient before coalescence. (*c*) Formation of bridge with very small and negative interface radius of curvature at the initiation of coalescence. Larger influx of liquid from the left drop causes contact angle at *A* to reduce and bridge to grow. When the contact angle at *A* reduces to the receding value whole of the liquid from left drop flows into the right drop. (*d*) State of drop just after coalescence. During coalescence, due to out flux of liquid, $\theta_{d,A}$ becomes smaller than receding contact, which is reflected at the edge *E* of the merged droplet. While at *D*, due to influx of liquid $\theta_{d,D}$ becomes greater than advancing contact angle: (*a*) drop on a surface with wettability gradient, (*b*) before coalescence, (*c*) during coalescence, and (*d*) after coalescence.

The effect of wettability gradient on dynamic contact angle has been described earlier [9,10,27] and we here present a brief review. When a drop is placed on a surface with wettability gradient, it takes a staggered spherical cap shape, as shown in Fig. 2. This results in a nonuniform curvature of liquid–vapor interface [9,10,27] and thus variation of Laplace pressure, $\Delta p(=2\gamma/r)$ within the drop. As the Laplace pressure inside the drop equalizes, the drop on a surface with low contact hysteresis takes a nearly spherical cap shape with uniform curvature [28], as shown in Fig. 2(*a*). The shift to spherical configuration creates nearly equal contact angle at its front and rear edge [9,10,28], that is at edges *A* and *B* of the drop shown in Fig. 2(*a*). For drop of sufficiently large size (as given by Eq. (6), the dynamic contact angle reduces to receding contact angle at *A* and increases to advancing contact angle at *B* and thus overcomes the resistance of hysteresis force. We note that variable curvature of drop (differential Laplace pressure) leading to spontaneous droplet motion has also been experimentally demonstrated by Lv et al. [29], Wang et al. [30], and Zheng et al. [31].

In contrast to wettability gradient, condensation of vapor increases the dynamic contact angle at both edge *A* and edge *B* of the drop [32]. Due to the vapor condensation and equalization of Laplace pressure, the dynamic contact angle takes average values of $\theta_{d,A}$ and $\theta_{d,B}$ at *A* and *B*, respectively, as shown in Fig. 2(*b*). The dynamic contact angle at *A*, $\theta_{d,A}$ becomes smaller than the ACA $\theta_{a,A}$ ($\angle aAB$) but is greater than the RCA $\theta_{r,A}$ ($\angle a'AB$) and therefore contact line at *A* neither recedes nor advances. However, the dynamic contact angle at *B*, $\theta_{d,B}$ becomes greater than the ACA $\theta_{a,B}$ ($\angle bBA$). Therefore, with further condensation, the contact line at *B* advances toward higher wettability region. Consequently, this moving contact line catches up with droplets condensing ahead of it initiating coalescence, as shown in Fig. 2(*c*).

The coalescence of drops proceeds through the formation of liquid bridge of very small and negative radius of curvature at the contact point. Typically, when two drops coalesce on a uniform wettability surface, equal quantities of liquid from both the drops rush toward the liquid bridge [33,34]. This motion of liquid toward the liquid bridge between the drops pulls the liquid–vapor interface radially inward causing the dynamic contact angle to decrease at points *A* and *D*. And when the dynamic contact angle reduces to RCA, both the drops start moving toward each other. Depending upon the wettability of the surface, the momentum developed during the process is either dissipated by viscous effects (high wetting surface) or results in spontaneous droplet jumping (superhydrophobic surfaces) [33–35].

Coalescence of drops occurring on a surface with wettability gradient, although following a similar process, differ in many aspects from that on uniform wettability surface. First, for drops of equal volume, the drop on relatively high wetting surface has lower curvature as compared to the drop on low wetting surface [21,36], as shown schematically in Fig. 2(*a*). Further, nucleation of drops is faster on high wetting surface as compared to low wetting surface, and therefore has higher volume [20]. Due to these effects, drops on high wetting surface have lower curvature and Laplace pressure than drops on low wetting surface, as shown in Fig. 2(*b*). This difference in the Laplace pressure causes larger volume of liquid to flow from drop on low wetting surface toward the liquid bridge. The unequal displacement of liquid from coalescing drops in turn leads to reduction of dynamic contact angle $\theta_{d,A}$ to RCA ($\theta_{r,A}$) prior to the similar reduction of dynamic contact angle $\theta_{d,D}$ for drop on high wetting surface. Prior reduction of dynamic contact angle to RCA is also aided by the fact that low wetting surface has lower hysteresis than the high wetting surface. The reduction of dynamic contact angle to RCA causes the whole drop on low wetting surface to move toward the liquid bridge. The momentum gained by the drop during the process pushes the drop past the contact point and into the drop on high wetting surface. The mass and momentum of the incoming liquid expand the liquid–vapor interface of the drop on high wetting surface, as shown by Lai et al. [36]. On a surface with low hysteresis (6 deg–7 deg), the expansion of the liquid–vapor interface makes the dynamic contact angle $\theta_{d,D}$ of the drop on high wetting surface greater than the ACA $\theta_{a,D}$ and thus unpins the three phase contact line, as shown in Fig. 2(*d*). And as a result, the merged drop begins to move. We note that, in the experiments of Lai et al., the contact angle hysteresis was 20 deg–25 deg. In effect, the coalescence aids the motion of drop by reducing the hysteresis. Above mechanism correctly explains the shift of center of mass of two coalescing drops on a surface with wettability gradient toward the drop on high wetting region observed experimentally by Zhao and Beysens [20] and Daniel et al. [10]. Besides, the mechanism of unpinning of contact line due to shape fluctuation of the drop is similar to the unpinning of drop contact line on a vibrating surface [26,37,38]. Lateral vibration of the surface holding the drop results in drop shape similar to the shape shown in Fig. 2(*d*), leading to drop motion. In our case, the fluctuations in the drop shape are induced by asymmetrical nature of drop coalescence.

The whole process of coalescence of two drops on a surface with contact angle gradient can be approximated as pumping of liquid from a drop on low wetting surface to a drop on high wetting surface. Here, we idealize each coalescence between two drops, by considering two equal size drops; such assumption is routinely applied in studies on drop coalescence [33,34]. Because of the length scales involved, the equilibrium shape of a droplet is approximated as spherical cap with an apparent contact angle θ_d. For a system, consisting of droplets of radius *r* placed on a solid substrate, the total surface energy can be expressed as $E=\gamma A_{lv}+\gamma_{sv}A_{sv}+\gamma_{sl}A_{sl}$, where subscripts *sv*, *sl*, and *lv* denote solid–vapor, solid–liquid and liquid–vapor interface, respectively, and *A* is the surface area [39].

When the two drops of radius *r* coalesce to form a new larger drop of radius *R*, the change in total surface energy is given by

$$\Delta E=\gamma\Delta A_{lv}-(\gamma\cos\theta_d)\,\Delta A_{sl} \tag{7}$$

where $\Delta A_{lv}=0.82\,\pi r^2(1-\cos\theta_d)$ and $\Delta A_{sl}=0.41\,\pi r^2\sin^2\theta_d$, respectively, are change in surface area of liquid vapor and solid–liquid interfaces (see derivation in Appendix). Differentiating Eq. (7) with respect to *r* gives the radial force acting on the interfaces of the two drops. Using the relation between base radius r_b and radius of curvature *r* of each drop prior to coalescence, $r_b=r/\sin\theta$ (see Fig. 2(*b*)), the resulting expression for force is given by

$$F_r=\frac{0.8\pi r_b\gamma_{lv}\left(2(1-\cos\theta_d)-\sin^2\theta_d\cos\theta_d\right)}{\sin\theta_d} \tag{8}$$

However, when two drops coalesce, some of the coalescence-released surface energy is dissipated due to viscous dissipation. The energy dissipated due to viscous effects can be approximated as [40–42]

$$E_{\text{vis}}=\int_0^{\tau_c}\int_\Omega \Phi d\Omega dt\approx\Phi\Omega\tau_c \tag{9}$$

where $\Omega=\pi r^3(2-3\cos\theta_d+\cos^3\theta_d)/3$ is volume of each drop, $\tau_c=\sqrt{\rho r^3/\gamma_{lv}}$ is the characteristic time scale of coalescence. Here, we note that characteristic time-scale τ_c is inertial capillary time scale. This is because for experimentally observed length scales of drop coalescence $\text{Re}>1$ [43]. In Eq. (9), $\Phi\approx 12\mu(U/r)^2$ [41] is the dissipation function, where μ is the viscosity and *U* is the average velocity of droplet liquid. As the two drops begin to coalesce, the capillary pressure Δp inside the drop drives the drops in horizontal direction. The average velocity *U* during the whole process of coalescence has been given by

Thoroddsen and Takehara [44] as $U \approx \tau_c \Delta p A_{\text{sec}}/\rho\Omega$, where $A_{\text{sec}} = r^2(\theta + \sin\theta\cos\theta_d)$ is cross section of the droplet and $\Delta p = 2\gamma_{lv}/r$.

Using the above expressions for volume of drop Ωr characteristic time-scale τ_c, dissipation function Φ, average velocity U, and cross section area A_{sec} in Eq. (9), energy dissipated due to viscous effects is given by

$$E_{\text{vis}} = 144\mu\sqrt{\frac{r^3\gamma}{\rho}}\frac{(\theta_d + \sin\theta_d\cos\theta_d)^2}{\pi(2 - 3\cos\theta_d + \cos^3\theta_d)} \tag{10}$$

Therefore, actual radial force on the droplet interface due to coalescence can be expressed as

$$F_a = \eta F_r, \quad \text{where, } \eta = \frac{\Delta E - E_{\text{vis}}}{\Delta E} \tag{11}$$

is coalescence efficiency.

As noted previously, force F_a on the interface of the drops acts to reduce the effect of hysteresis. We note that the coalescence efficiency η depends on local wetting condition and radius of the coalescing drops. For coalescence released energy to be effective, the coalescence efficiency must be positive ($\eta > 0$). Accounting for the force due to coalescence in overcoming hysteresis force, Eq. (6) modifies to

$$\pi r_b^2\gamma\frac{d(\cos\theta_d)}{dx} - (2\gamma r_b(\cos\theta_{ro} - \cos\theta_{ao}) - F_a) = 0 \tag{12}$$

Solving Eq. (12) for base radius r_b gives the radius $r_{\max}$ at which drops start departing from the condensation surface. We note that Eq. (12) is fourth-order polynomial equation in r and there is no explicit analytical solution for $r_{\max}$. Therefore, Eq. (12) is solved numerically to find drop departure radius $r_{\max}$. Also, the maximum drop radius $r_{\max}$ obtained from Eq. (12) is the radius of the drops prior to coalescence (see Fig. 2(*b*)). If we assume that nucleation sites have a uniform distribution over the surface and form a square array then, $r_e = (4N_s)^{-1/2}$, where N_s is number of nucleation sites per unit area of condensation surface. Using the boundary condition ($n(r_e) = N(r_e)$) drop size distribution of small drop, obtained after integration of Eq. (3), is expressed as

$$n(r) = \frac{1}{3\pi r_e^3 r_{\max}}\left(\frac{r_{\max}}{r_e}\right)^{2/3}\frac{r}{C}\frac{A_2 r + A_3}{A_2 r_e + A_3}\exp(B) \tag{13}$$

where

$$B = \frac{A_2}{\tau A_1}\left[\frac{r_e^2 - r^2}{2} + r_{\min}C - r_{\min}^2\ln D\right] + \frac{A_3}{\tau A_1}[C - r_{\min}\ln D] \tag{14}$$

$C = r_e - r$, $D = (r - r_{\min})/(r_e - r_{\min})$, $A_1 = \Delta T(1 - \cos\theta)/(2 - 3\cos\theta + \cos^3\theta)\rho h_{fg}$, $A_2 = \theta(1 - \cos\theta)/4K_c\sin\theta$ and $A_3 = \delta(1 - \cos\theta)/(K_{\text{coat}}\sin^2\theta) + 1/2h_i$ [8]. Also, from the empirical relation given by Lefevre and Rose [25] for the drop size distribution of large drops $N(r)$, we have

$$N(r) = \frac{1}{3\pi r^2 r_{\max}}\left(\frac{r}{r_{\max}}\right)^{-2/3} \tag{15}$$

Taking logarithm of this equation, we get

$$\ln(N(r)) = \ln\left(\frac{1}{3\pi r_{\max}^{1/3}}\right) - \frac{8}{3}\ln r \tag{16}$$

Next, differentiating Eq. (16) with respect to $\ln(r)$, we get

$$\frac{d\ln(N(r))}{d\ln(r)} = -\frac{8}{3} \tag{17}$$

Applying this condition at $r = r_e$, gives [8,18]

$$\frac{d(\ln n(r))}{d(\ln r)} = \frac{d(\ln N(r))}{d(\ln r)} = -\frac{8}{3} \tag{18}$$

Equation (18) enables the sweeping period τ to be expressed as [8,18]

$$\tau = \frac{3r_e^2(A_2 r_e + A_3)^3}{A_1(11A_2 r_e^2 - 14A_2 r_e r_{\min} + 8A_3 r_e - 11A_3 r_{\min})} \tag{19}$$

To model the surface with wettability gradient, entire condensation surface is divided into m parts of equal width in the direction of wettability gradient. We assume contact angle variation of the form $\cos\theta_d = I + Sx$, where x is the spatial coordinate along the wettability gradient from low wetting to high wetting end. Using Eq. (1), we calculate heat flux in each segment. After that, we numerically integrate the heat transfer in each segment to get the total dropwise condensation heat transfer.

3 Results and Discussion

3.1 Dropwise Condensation Heat Flux. To validate our model, we begin by comparing DWC heat flux predictions with experiments of Daniel et al. [10] and a related study by Chaudhury et al. [21]. In these experiments, DWC heat flux was measured on a disk-shaped horizontal surface having a radius of 0.5 cm. The top surface of the disk is treated chemically to obtain radial wettability gradient such that the contact angle decreases from center to outer periphery. The contact angle varies from 100 deg at the center to nearly 20 deg at the outer periphery with contact angle hysteresis of 6 deg. As described in Sec. 2.3, to model the surface with wettability gradient, the entire condensing surface is divided radially into m =100 equal parts.

In Fig. 3, we present ideal DWC heat flux at various degrees of subcooling and its comparison with experimental results of Chaudhury et al. [21]. For these calculation, we take nucleation site density $N_s = 1 \times 10^{10}\,\text{m}^{-2}$ [17], thickness of the coating layer $\delta = 100$ nm, $T_{\text{sat}} = 373$ K, and conductivity of coating layer $K_{\text{coat}} = 2\,\text{Wm}^{-1}\text{K}^{-1}$ [45]. Further, we used thermophysical properties of working fluid (water) from NIST chemistry webbook [46]. The theoretical predictions agree well with the experimental results of Chaudhury et al. for degree of subcooling $\Delta T < 4$ K at which most of the reliable data is considered to be recorded [4]. Also, the Nusselt number

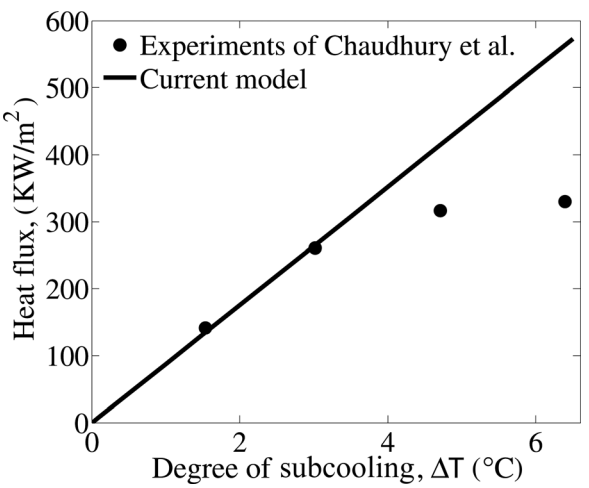

Fig. 3 Comparison of heat flux predicted by our mathematical model with the experimental results [10,21] as a function degree of subcooling. The calculations are based on nucleation site density, $N_s = 1\times10^{10}\text{m}^{-2}$, $T_{\text{sat}} = 373$ K, $\delta = 100$ nm.

predicted by our model for $\Delta T < 4$ K is Nu = 6450, taking thermal conductivity of the water to be 0.69 $Wm^{-1}K^{-1}$. This is in good agreement with Nu = 6700 obtained experimentally by Daniel et al. [10]. Note that most of the applications depending on condensation process practically operate at $\Delta T < 4$ K [47,48]. At degree of subcooling greater than 4 K, experimental results deviate from the theoretical predictions. The deviation of experimental results from DWC theory is attributed to the beginning of transition regime [4–7], analogous to the transition from nucleate to film boiling.

3.2 Steady-State Drop Size Distribution. The steady-state normalized drop size distribution obtained from the present theoretical model and the experimental study of Macner et al. [11] is presented in Fig. 4. Macner et al. performed condensation on the underside of a horizontal disk (radius 6 mm), which was treated chemically to obtain wettability gradient. The test surface had uniform contact angle up to a distance of 3 mm from the center (30% of area) and continuous wettability gradient from 3 mm to 6 mm with contact angle varying from 95 deg to 50 deg. In their experiments, Macner et al. observed that the drop size distribution on a surface with wettability gradient remained steady due to frequent sweeping of the drops. Furthermore, they observed that the drops in the high-wetting part of the surface are larger in size than the drops on low wetting surface. The drop size distributions are normalized by highest drop population occurring in the respective drop size distributions. The highest drop population density was found near drop radius of 80 μm. We note that, due to the limitations posed by optical instruments, Macner et al. were only able to observe drops of radius larger than 80 μm. Therefore, as per the experimental study, the distribution of droplet population is presented for drop size, $r > 80$ μm. Theoretical drop size distribution follows similar trend and compares well with the experimental data. The small discrepancy at higher drop sizes can be attributed to the existence of surface with uniform contact angle. On such a surface, drops are removed at capillary length scale ($r \sim \mathcal{O}(1\text{mm})$). As a result, most of the area is covered by drops of size closer to capillary length (≈2.4 mm) and correspondingly have lower population of small drops ($r \sim \mathcal{O}(80\ \mu\text{m})$) and higher population of large drops ($r \sim \mathcal{O}(100 - 1000\ \mu\text{m})$. Such behavior of drop size distribution is also evident from the experimental results of Macner et al. In contrast to uniform wetting surface, drop departure size vary along the gradient on a surface with wettability gradient and most drops are removed at length scales much smaller than the capillary length. And therefore surface with wettability gradient have higher population of small drops as compared to large drops.

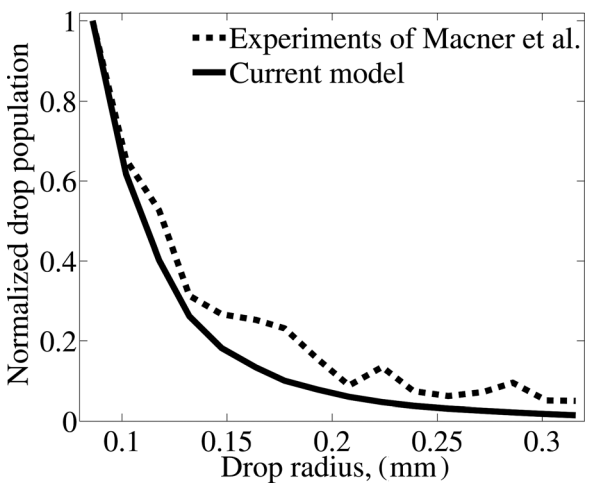

Fig. 4 Comparison of drop size distribution predicted by our mathematical model with the experimental results of Macner et al. [11]. The distributions are plotted for drops with radius, $r \geq 80$ μm. These calculations are performed for nucleation site density, $N_s = 1\times10^{10}\text{m}^{-2}$, $T_{sat} = 373$ K, $\delta = 100$ nm.

3.3 Effect of Wettability Gradient on Dropwise Condensation Heat Flux. In Fig. 5(*a*), we show the effect of wettability gradient on DWC heat flux. For these calculations, we considered a surface of dimensions identical to the surface used in experimental study by Daniel et al. [10] and described in Sec. 3.1. We perform the calculations for degree of subcooling $\Delta T = 2$ K, nucleation site density $N_s = 1 \times 10^{10}\,\text{m}^{-2}$ [17], thickness of the coating layer $\delta = 100$ nm, $T_{sat} = 373$ K, and conductivity of coating layer $K_{coat} = 2\,\text{Wm}^{-1}\text{K}^{-1}$. To illustrate the effect of wettability gradient, we have chosen surfaces with wettability gradients of 20 deg–80 deg, 20 deg–90 deg, 20 deg–100 deg, 20 deg–120 deg, and 20 deg–150 deg. The first value in above notation, for example, in 20 deg–80 deg, denotes the contact angle at the periphery and the later denote the contact angle at the center of the disk. Heat flux first increases and then decreases with an increase in wettability gradient. Heat flux, as shown in Fig. 1, is governed by population density $n(r)$ and heat transfer $q_d(r)$ through a drop of radius r. The population density is a function of r_{max} (smaller the r_{max} higher is the population density), which in turn is a function

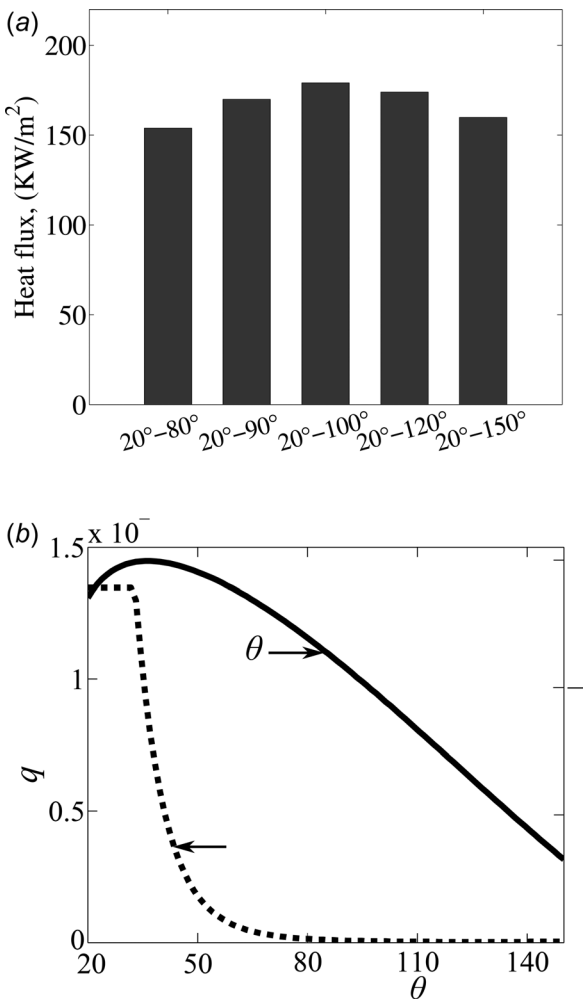

Fig. 5 Effect of wettability gradient on DWC heat flux and size of drop departure. (*a*) DWC heat flux at different wettability gradients while keeping the minimum contact angle constant. (*b*) Variation in size of drop departure and heat transfer through a drop with contact angle for the largest wettability gradient 20 deg–150 deg. These calculations are performed for nucleation site density, $N_s = 1\times10^{10}\,\text{m}^{-2}$, $T_{sat} = 373$ K, $\delta = 100$ nm.

contact angle and wettability gradient. Figure 5(*b*) shows the variation of drop departure radius r_{max} and heat transfer through a drop q_d with contact angle corresponding to highest wettability gradient 20 deg–150 deg. Increasing the contact angle and thus the wettability gradient leads to monotonous decrease in r_{max}. However, the decrease in r_{max} is only marginal for contact angle greater than 100 deg. In contrast, heat transfer through a drop decreases linearly for drops with contact angle $\theta > 100$ deg [8], as shown in Fig. 5(*b*). Therefore, for increase in wettability gradient from 20 deg–80 deg to 20 deg–100 deg, gain in population density dominates over decrease in heat transfer through a drop. Whereas, for increase in wettability gradient from 20 deg–100 deg to 20 deg–150 deg, small gain population density is offset by reduced heat transfer through drops resulting in decreased heat flux.

3.4 Effect of Thickness of Coating Layer. Almost all natural surfaces have uniform wettability. To create a surface with wettability gradient, surface is coated, through chemical treatment, with a layer of promoter coating. This layer of coating acts as an additional layer of thermal resistance between vapor and surface. Additional resistance due to the thickness of the coating layer does not affect the drop size distribution; however, it plays a vital role in the heat transfer through a drop (Eq. (2)). In Fig. 6, we show the effect of thickness of coating layer on heat transfer through a drop and thus DWC heat transfer on surface with wettability gradient. We perform the calculations for degree of subcooling $\Delta T = 2$ K, $T_{sat} = 373$ K and conductivity of coating layer $K_{coat} = 2\,\mathrm{Wm^{-1}K^{-1}}$. As expected, with an increase in the thickness of coating layer, heat transfer through a drop decreases leading to decrease in DWC condensation heat flux. However, from Fig. 6, we see that the rate of heat transfer through a drop peaks at a certain contact angle. The contact angle at which the maximum heat transfer rate is attained varies with the coating thickness. For example, the contact angle at which there is maximum rate of heat transfer through a drop changes to 80 deg for $\delta = 10$ μm from 40 deg for $\delta = 0.1$ μm (see Fig. 6). Because of the reasons mentioned in Sec. 3.3, this change in contact angle corresponding to maximum rate of heat transfer through a drop in turn changes the optimal choice of wettability gradient. Performing the calculations discussed in Sec. 3.3 again for $\delta = 10$ μm yields the optimal wettability gradient to be 20 deg–110 deg in contrast to 20 deg–100 deg for $\delta = 0.1$ μm.

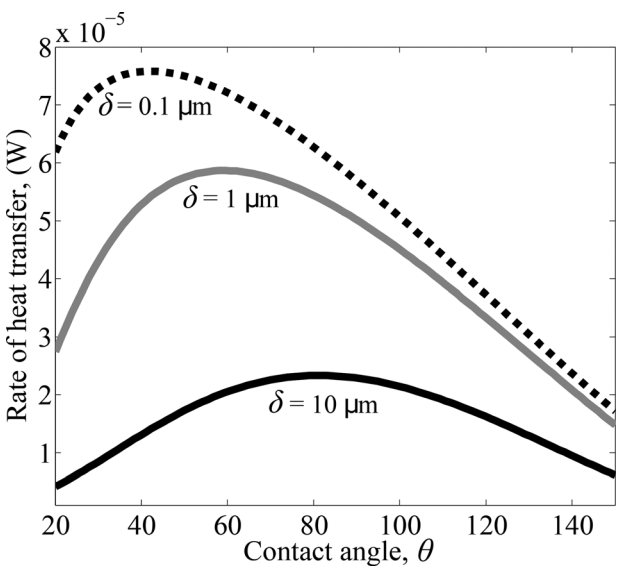

Fig. 6 Effect of thickness of coating layer δ on heat transfer through a drop. These calculations are performed for degree of subcooling $\Delta T = 2$ K, $r = 5$ μm, $T_{sat} = 373$ K and conductivity of coating layer $K_{coat} = 2\,\mathrm{Wm^{-1}K^{-1}}$.

4 Conclusion

We have developed a mathematical model based on population balance to predict the DWC heat transfer on a surface with wettability gradient. The model takes into account the effect of wettability gradient and energy released during drop coalescence to determine drop departure size. We validated our model with published experimental data of dropwise condensation heat flux and drop size distribution. Our model is applicable for potential applications of DWC in steam power plants, water desalination, and water collection wherein degree of subcooling is low. However, our model is not applicable at high degree of subcooling where transition regime characterized by partial DWC and partial FWC sets in. In future, we will extend our model to include the effect of partial FWC so as to model the transition regime. Based on various experimental studies, we also proposed a mechanism by which coalescence released surface energy aids droplet motion. We propose that, due to asymmetrical nature of drop coalescence on a surface with wettability gradient, shape fluctuations similar to drop on a vibrating surface are induced. As a result of these fluctuations, dynamic contact angle of the drop approaches ACA at one edge and RCA at other and thus the drop begins to move. Based on the mathematical model, we evaluated the effect of wettability gradient on DWC heat flux for a surface of given dimensions. With the minimum contact angle kept constant, DWC heat flux first increases and then decreases with an increase in wettability gradient. For thickness of coating layer $\delta = 100$ nm, DWC heat flux decreases when part of the surface has wettability greater than 100 deg. For regions with contact angle greater than 100 deg, reduction in heat transfer through a drop dominates any gain in population density due to low wettability. Lastly, we demonstrated that the optimal choice of wettability gradient also depends on the thickness of coating layer and varies with change in coating thickness.

Acknowledgment

S. K. thanks DST INSPIRE fellowship for providing necessary funds for carrying out this research.

Appendix

Here, we provide the derivation for change in the area of solid–liquid and liquid–vapor interface due to coalescence of two equal size drops. Let r be the radius of the drops prior to coalescence and R the radius merged drop. The volume of each of the two coalescing drops V_d is given by

$$V_d = \pi r^3(2 - 3\cos\theta + \cos^3\theta)/3 \tag{A1}$$

and the volume of the drop resulting from coalescence of two equal size drops V_c is given by

$$V_c = \pi R^3(2 - 3\cos\theta + \cos^3\theta)/3 \tag{A2}$$

From mass conservation, we must have $2V_d = V_c$. That is

$$2\pi r^3(2 - 3\cos\theta + \cos^3\theta)/3 = \pi R^3(2 - 3\cos\theta + \cos^3\theta)/3 \tag{A3}$$

from this equation, we get $R = 2^{1/3}r$. Because the base radius each of the two drops prior to coalescence is $r\sin\theta$ and that of the merged drop is $R\sin\theta$, the change to total base area due to coalescence is given by

$$\Delta A_{sl} = 2\pi r^2 \sin^2\theta - \pi R^2 \sin^2\theta \tag{A4}$$

Finally, substituting $R = 2^{1/3}r$ in this relation, we get the desired expression of change in solid–liquid interface ΔA_{sl} as

$$\Delta A_{sl} = 0.41\,\pi r^2 \sin^2\theta \tag{A5}$$

Next, the liquid–vapor interface area of each of the drops prior to the coalescence ΔA_{lvd} is given by

$$\Delta A_{lvd} = 2\pi r^2(1 - \cos\theta) \tag{A6}$$

Similarly, the liquid–vapor interface area of the merged drop ΔA_{lvc} is given by

$$\Delta A_{lvc} = 2\pi R^2(1 - \cos\theta) \tag{A7}$$

Now, change in liquid–vapor interface due to coalescence is $\Delta A_{lv} = 2\Delta A_{lvd} - \Delta A_{lvc}$. That is

$$\Delta A_{lv} = 4\pi r^2(1 - \cos\theta) - 2\pi R^2(1 - \cos\theta) \tag{A8}$$

Substituting $R = 2^{1/3}r$ in this expression gives the change in liquid–vapor interface area ΔA_{lv} as

$$\Delta A_{lv} = 0.82\,\pi r^2(1 - \cos\theta) \tag{A9}$$

References

[1] Schmidt, E., Schurig, W., and Sellschopp, W., 1930, "Versuche Über Die Kondensation Von Wasserdampf in Film-Und Tropfenform," Tech. Mech. Thermodyn., **1**(2), pp. 53–63.
[2] Le Fevre, E., and Rose, J., 1965, "An Experimental Study of Heat Transfer by Dropwise Condensation," Int. J. Heat Mass Transfer, **8**(8), pp. 1117–1133.
[3] Graham, C., and Griffith, P., 1973, "Drop Size Distributions and Heat Transfer in Dropwise Condensation," Int. J. Heat Mass Transfer, **16**(2), pp. 337–346.
[4] Rose, J., 2002, "Dropwise Condensation Theory and Experiment: A Review," Proc. Inst. Mech. Eng., Part A: J. Power Energy, **216**(2), pp. 115–128.
[5] Tanasawa, I., and Utaka, Y., 1983, "Measurement of Condensation Curves for Dropwise Condensation of Steam at Atmospheric Pressure," ASME J. Heat Transfer, **105**(3), pp. 633–638.
[6] Stylianou, S., and Rose, J., 1983, "Drop-to-Filmwise Condensation Transition: Heat Transfer Measurements for Ethanediol," Int. J. Heat Mass Transfer, **26**(5), pp. 747–760.
[7] Patankar, N. A., 2010, "Supernucleating Surfaces for Nucleate Boiling and Dropwise Condensation Heat Transfer," Soft Matter, **6**(8), pp. 1613–1620.
[8] Kim, S., and Kim, K. J., 2011, "Dropwise Condensation Modeling Suitable for Superhydrophobic Surfaces," ASME J. Heat Transfer, **133**(8), p. 081502.
[9] Greenspan, H. P., 1978, "On the Motion of a Small Viscous Droplet That Wets a Surface," J. Fluid Mech., **84**(1), pp. 125–143.
[10] Daniel, S., Chaudhury, M. K., and Chen, J. C., 2001, "Fast Drop Movements Resulting From the Phase Change on a Gradient Surface," Science, **291**(5504), pp. 633–636.
[11] Macner, A. M., Daniel, S., and Steen, P. H., 2014, "Condensation on Surface Energy Gradient Shifts Drop Size Distribution Toward Small Drops," Langmuir, **30**(7), pp. 1788–1798.
[12] Ashley, K. M., Meredith, J. C., Amis, E., Raghavan, D., and Karim, A., 2003, "Combinatorial Investigation of Dewetting: Polystyrene Thin Films on Gradient Hydrophilic Surfaces," Polymer, **44**(3), pp. 769–772.
[13] Choi, S.-H., and Zhang Newby, B.-M., 2003, "Micrometer-Scaled Gradient Surfaces Generated Using Contact Printing of Octadecyltrichlorosilane," Langmuir, **19**(18), pp. 7427–7435.
[14] Huang, Z., Zhang, J., Cheng, J., Xu, S., Pi, P., Cai, Z., Wen, X., and Yang, Z., 2012, "Preparation and Characterization of Gradient Wettability Surface Depending on Controlling Cu (Oh) 2 Nanoribbon Arrays Growth on Copper Substrate," Appl. Surf. Sci., **259**, pp. 142–146.
[15] Sommers, A., Brest, T., and Eid, K., 2013, "Topography-Based Surface Tension Gradients to Facilitate Water Droplet Movement on Laser-Etched Copper Substrates," Langmuir, **29**(38), pp. 12043–12050.
[16] Tanaka, H., 1975, "A Theoretical Study of Dropwise Condensation," ASME J. Heat Transfer, **97**(1), pp. 72–78.
[17] Leach, R., Stevens, F., Langford, S., and Dickinson, J., 2006, "Dropwise Condensation: Experiments and Simulations of Nucleation and Growth of Water Drops in a Cooling System," Langmuir, **22**(21), pp. 8864–8872.
[18] Abu-Orabi, M., 1998, "Modeling of Heat Transfer in Dropwise Condensation," Int. J. Heat Mass Transfer, **41**(1), pp. 81–87.
[19] Ranodolph, A., 2012, *Theory of Particulate Processes 2e: Analysis and Techniques of Continuous Crystallization*, Elsevier, London.
[20] Zhao, H., and Beysens, D., 1995, "From Droplet Growth to Film Growth on a Heterogeneous Surface: Condensation Associated With a Wettability Gradient," Langmuir, **11**(2), pp. 627–634.
[21] Chaudhury, M. K., Chakrabarti, A., and Daniel, S., 2015, "Generation of Motion of Drops With Interfacial Contact," Langmuir, **31**(34), pp. 9266–9281.
[22] Tanaka, H., 1975, "Measurements of Drop-Size Distributions During Transient Dropwise Condensation," ASME J. Heat Transfer, **97**(3), pp. 341–346.
[23] Maa, J. R., 1978, "Drop Size Distribution and Heat Flux of Dropwise Condensation," Chem. Eng. J., **16**(3), pp. 171–176.
[24] Sikarwar, B. S., Battoo, N. K., Khandekar, S., and Muralidhar, K., 2011, "Dropwise Condensation underneath Chemically Textured Surfaces: Simulation and Experiments," ASME J. Heat Transfer, **133**(2), p. 021501.
[25] LeFevre, E., and Rose, J., 1966, "A Theory of Heat Transfer by Dropwise Condensation," Third International Heat Transfer Conference, Chicago, IL, Aug. 7–12, pp. 362–375.
[26] Daniel, S., and Chaudhury, M. K., 2002, "Rectified Motion of Liquid Drops on Gradient Surfaces Induced by Vibration," Langmuir, **18**(9), pp. 3404–3407.
[27] Brochard, F., 1989, "Motions of Droplets on Solid Surfaces Induced by Chemical or Thermal Gradients," Langmuir, **5**(2), pp. 432–438.
[28] Ito, Y., Heydari, M., Hashimoto, A., Konno, T., Hirasawa, A., Hori, S., Kurita, K., and Nakajima, A., 2007, "The Movement of a Water Droplet on a Gradient Surface Prepared by Photodegradation," Langmuir, **23**(4), pp. 1845–1850.
[29] Lv, C., Chen, C., Chuang, Y.-C., Tseng, F.-G., Yin, Y., Grey, F., and Zheng, Q., 2014, "Substrate Curvature Gradient Drives Rapid Droplet Motion," Phys. Rev. Lett., **113**(2), p. 026101.
[30] Wang, Q., Yao, X., Liu, H., Quéré, D., and Jiang, L., 2015, "Self-Removal of Condensed Water on the Legs of Water Striders," Proc. Natl. Acad. Sci. U.S.A., **112**(30), pp. 9247–9252.
[31] Zheng, Y., Bai, H., Huang, Z., Tian, X., Nie, F.-Q., Zhao, Y., Zhai, J., and Jiang, L., 2010, "Directional Water Collection on Wetted Spider Silk," Nature, **463**(7281), pp. 640–643.
[32] Anand, S., and Son, S. Y., 2010, "Sub-Micrometer Dropwise Condensation Under Superheated and Rarefied Vapor Condition," Langmuir, **26**(22), pp. 17100–17110.
[33] Nam, Y., Kim, H., and Shin, S., 2013, "Energy and Hydrodynamic Analyses of Coalescence-Induced Jumping Droplets," Appl. Phys. Lett., **103**(16), p. 161601.
[34] Liu, F., Ghigliotti, G., Feng, J. J., and Chen, C.-H., 2014, "Numerical Simulations of Self-Propelled Jumping upon Drop Coalescence on Non-Wetting Surfaces," J. Fluid Mech., **752**, pp. 39–65.
[35] Boreyko, J. B., and Chen, C.-H., 2009, "Self-Propelled Dropwise Condensate on Superhydrophobic Surfaces," Phys. Rev. Lett., **103**(18), p. 184501.
[36] Lai, Y.-H., Hsu, M.-H., and Yang, J.-T., 2010, "Enhanced Mixing of Droplets During Coalescence on a Surface With a Wettability Gradient," Lab Chip, **10**(22), pp. 3149–3156.
[37] Brunet, P., Eggers, J., and Deegan, R., 2007, "Vibration-Induced Climbing of Drops," Phys. Rev. Lett., **99**(14), p. 144501.
[38] Noblin, X., Kofman, R., and Celestini, F., 2009, "Ratchetlike Motion of a Shaken Drop," Phys. Rev. Lett., **102**(19), p. 194504.
[39] De Gennes, P.-G., Brochard-Wyart, F., and Quéré, D., 2013, *Capillarity and Wetting Phenomena: Drops, Bubbles, Pearls, Waves*, Springer Science & Business Media, New York.
[40] Chandra, S., and Avedisian, C., 1991, "On the Collision of a Droplet With a Solid Surface," Proc. R. Soc. A, **432**(1884), pp. 13–41.
[41] Wang, F.-C., Yang, F., and Zhao, Y.-P., 2011, "Size Effect on the Coalescence-Induced Self-Propelled Droplet," Appl. Phys. Lett., **98**(5), p. 053112.
[42] Lv, C., Hao, P., Yao, Z., Song, Y., Zhang, X., and He, F., 2013, "Condensation and Jumping Relay of Droplets on Lotus Leaf," Appl. Phys. Lett., **103**(2), p. 021601.
[43] Aarts, D. G., Lekkerkerker, H. N., Guo, H., Wegdam, G. H., and Bonn, D., 2005, "Hydrodynamics of Droplet Coalescence," Phys. Rev. Lett., **95**(16), p. 164503.
[44] Thoroddsen, S., and Takehara, K., 2000, "The Coalescence Cascade of a Drop," Phys. Fluids, **12**(6), pp. 1265–1267.
[45] Yaws, C. L., 1995, *Handbook of Thermal Conductivity, Volume 3: Organic Compounds C8 to C28*, Vol. 3, Gulf Professional Publishing, Houston, TX.
[46] Lemmon, E., McLinden, M., and Friend, D., 2005, "Thermophysical Properties of Fluid Systems," *NIST Chemistry WebBook, SRD 69*, National Institute of Standards and Technology, Gaithersburg, MD.
[47] Vosough, A., Falahat, A., and Vosough, S., 2011, "Improvement Power Plant Efficiency With Condenser Pressure," Int. J. Multidiscip. Sci. Eng., **2**(3), pp. 38–43.
[48] Sikarwar, A. S., Dandotiya, D., and Agrawal, S. K., 2013, "Performance Analysis of Surface Condenser Under Various Operating Parameters," Int. J. Eng. Res. Appl., **3**(4), pp. 416–421.